Journal of Power Sources 196 (2011) 5317–5324

Contents lists available at ScienceDirect

Journal of Power Sources

journal homepage: www.elsevier.com/locate/jpowsour

Estimation of water distribution and degradation mechanisms in polymer electrolyte membrane fuel cell gas diffusion layers using a 3D Monte Carlo model

K. Seidenberger*, F. Wilhelm, T. Schmitt, W. Lehnert[1], J. Scholta

Zentrum für Sonnenenergie- und Wasserstoff-Forschung Baden-Württemberg, Helmholtzstraße 8, 89081 Ulm, Germany

ARTICLE INFO

Article history:
Received 21 July 2010
Accepted 24 August 2010
Available online 26 September 2010

Keywords:
Fuel cell
GDL degradation
Water management
Monte Carlo model

ABSTRACT

Understanding of both water management in PEM fuel cells and degradation mechanisms of the gas diffusion layer (GDL) and their mutual impact is still at least incomplete. Different modelling approaches contribute to gain deeper insight into the processes occurring during fuel cell operation. Considering the GDL, the models can help to obtain information about the distribution of liquid water within the material. Especially, flooded regions can be identified, and the water distribution can be linked to the system geometry. Employed for material development, this information can help to increase the life time of the GDL as a fuel cell component and the fuel cell as the entire system. The Monte Carlo (MC) model presented here helps to simulate and analyse the water household in PEM fuel cell GDLs. This model comprises a three-dimensional, voxel-based representation of the GDL substrate, a section of the flowfield channel and the corresponding rib. Information on the water distribution within the substrate part of the GDL can be estimated.

1. Introduction

One of the main obstacles on the way of polymer electrolyte membrane fuel cells (PEMFCs) towards commercial use is their durability. Thus during the last years a significant amount of research work has been done to investigate PEMFC degradation mechanisms and mitigation strategies. Up-to-date overviews on PEMFC degradation are given in [1–4]. For a long time the focus has been less on GDL ageing but different studies concerning the lifetime of fuel cells have rather investigated reaction layer, membrane and bipolar plate ageing. Nevertheless, recent results show that GDL degradation should not be neglected anymore. For the case of the electrode in [5] it was demonstrated that the degradation of the PTFE results in approximately two times higher performance losses than the catalyst degradation by Pt agglomeration after 1000 operating hours under the operating conditions chosen; this at least implies that an impaired water household caused by the loss of GDL hydrophobicity may have similarly severe effects. Though the correlation between liquid water and GDL degradation has been discussed since quite some time [6], the mechanisms are still not well understood. In principle two reasons of degradation for the PEMFC GDL are presumed:

- Changes of the wetting behaviour of the GDL: The wetting behaviour changes may be induced by PTFE decomposition, see e.g. [7], or depletion caused by oxidation of the PTFE or the carbon, mechanical effects [8] (compression or fibre cracking) or impurities [6]. By these effects the originally hydrophobic GDL becomes more hydrophilic which results in an accumulation of liquid water in the GDL pores and blocking of these pores for reactant transport.
- Changes of the structure of the GDL caused by mechanical effects (compression below the ribs, see [8,9]) or carbon oxidation (for the case of the MEA, see e.g. [10]) could change the electric as well as the heat conductivity of the GDL.

These mechanisms are not limited just to the GDL, but also influence other components of the PEM fuel cell. This phenomenon demonstrates how important the interaction of the different degradation mechanisms is. The changes in the wetting behaviour and the structure of the GDL and thus its durability depend on the operating conditions of the PEM fuel cell. In [11] it is stated that the presence of liquid water, excess reactants and high current densities induces significant degradation of the MEA and the GDL. The authors of [11,12] observe that high humidification and especially liquid water are correlated with PTFE decomposition.

The task of modelling the GDL water household implies two challenges: finding an appropriate description of the porous structure and modelling the dynamic behaviour of water and gas within this structure. In literature, different modelling approaches can be found associated with porous media description and modelling of

* Corresponding author. Tel.: +49 731 9530 208; fax: +49 731 9530 666.
E-mail address: katrin.seidenberger@zsw-bw.de (K. Seidenberger).
[1] Present address: Institut für Energieforschung - Brennstoffzellen (IEF-3), Forschungszentrum Jülich GmbH, 52425 Jülich, Germany.

0378-7753/$ – see front matter © 2010 Elsevier B.V. All rights reserved.
doi:10.1016/j.jpowsour.2010.08.068

transport phenomena in porous media. On the one hand there are several approaches to find a reasonable description of the porous media, on the other hand there are approaches to model the transport processes in porous media by solving macroscopic transport equations or by describing molecular particle transport. The former can be divided into models representing the real geometry of the porous structure, statistically generated structures, randomly generated structures, abstracted structures representing certain properties of the real material; even continuous material linked with some integral structural parameters as permeability can be used to describe transport properties of porous structures.

1.1. Macroscopic transport models

As an example for a macroscopic modelling approach, computational fluid dynamics (CFD) can be mentioned. This approach can be subdivided into two major categories. The first category is considering the real multi-fluid approach where the entire set of conservation equations for each phase is solved and the coupling of the equations is achieved through pressure and inter-phase exchange coefficients. A successful example of an implementation can be found in [13]. The second category is the multi-phase mixture approach where the mixture momentum equations are solved and the relative velocities are calculated in a post-iterative step. One of the first papers introducing this approach is [14]. In the context of CFD, the porous material can be described both by real geometry data or continuously together with integral structural parameters.

A further approach which has been successfully applied to the field is the Lattice Boltzmann (LB) method which indirectly solves the Navier–Stokes equation by dealing with the Boltzmann equation for fluid particle movement [15]. It works on a lattice consisting of equally shaped unit volumes (so-called lattice sites, or cells), which are either solid or filled with fluid.

Pore network models are designed to capture the transport properties, but not the morphology of porous media, i.e. they use abstracted structures to represent the properties of the pore space. The use of networks of capillary tubes to model porous media was first suggested in [16].

1.2. Nano- and microscopic models

Models based on macroscopic liquid properties may be useful up to at least the μm scale. Going to even smaller structures, e.g. the nm-scale pores within the MPL material of a fuel cell GDL, the model assumptions break down and fluid flow must be described on the basis of appropriate particle interactions. Molecular dynamics (MD) modelling is one of the principal tools to theoretically study fluid flow based on molecular interactions. This computational method describes the time dependent behaviour of a molecular system, thereby calculating particle interactions either using empirical forcefields or even quantum mechanical methods. Commonly, to describe particle movement, the classical equations of motion are integrated based on an adequate discretization in time. The MD method has been routinely used to investigate the structure, dynamics and thermodynamics of fluids. With MD simulations one can, e.g. study both thermodynamic properties and/or time dependent (kinetic) phenomena such as fluid flow in porous material (for a review, see [17–20]).

A further method which has been commonly used on the molecular scale is the Monte Carlo (MC) method, which was first described in [21]. Since then, MC simulations have been used in several fields of scientific modelling. Concerning fluid behaviour, some authors focus on phase change as [22] or on two phase flow without phase change as for example [23]. But also percolation theory [24] and diffusion, including Knudsen diffusion, [25] are considered. For all of these models, a proper representation mirroring the structure of the porous medium has to be found first. Therefore, depending upon the physical model to be used, simple 2D cylindrical pores as in [22] or spherical clusters as in [25] are employed.

Furthermore, the MC method has been used to gain a representation of the structure of porous media and the associated effective properties (see [22–29]). Some of the MC models also focus on the determination of general parameters of porous media, e.g. in [28] and [29], the MC simulation is used to compute the effective diffusivities in randomly overlapping fibres and filament bundles representing a porous medium. Further articles especially focus on fuel cell topics: in [26], electrical conduction aspects are examined, in [27], the MC method is used to generate the geometry for a lattice Boltzmann calculation of the permeability.

There are further particle-based models using not explicitly molecular, but small-scale descriptions of material behaviour. These include randomly distributed, overlapping grains such as oblate and prolate spheroids. They are known to quite accurately describe the pore space in sandstone, foams and fibre networks [30–33].

The novel approach presented in this article employs the MC method not on the molecular, but on the μm scale to describe water behaviour within randomly generated porous material on a statistical basis, i.e. without the need of numerically solving transport equations. Also real geometry data could be used.

1.3. Experimental visualization of water in PEMFC GDLs

Experimental in situ visualization of liquid water within PEMFCs has been approached using, e.g. optical imaging [34], neutron radiography and tomography [35], synchrotron radiography or tomography. Combined optical imaging and neutron radiography studies have been performed [36], but the spatial resolution of this technique is too low to gain insight into inner-GDL processes. Employing synchrotron radiography, e.g. Manke et al. [37] and Hartnig et al. [38] have shown that in situ water distributions within fuel cell GDLs of appropriate resolution can also be obtained in through-plane direction. Unfortunately, to our knowledge, so far no according experimental data dealing with ageing or variation of PTFE coverage is available.

Clearly, the experimental progress on the field opens new perspectives concerning water household analysis. Nevertheless, further effort on the field of theoretical modelling is required to provide and facilitate deeper understanding and to relieve material improvement by predicting the consequences of changing parameters. The MC model described in the following is intended to complement the established tools in this field.

This article is structured in the following way: first the MC model developed to study the water distribution in fuel cells will be described. Also model specific properties as the handling of porous media and the steady state as approximation of real fuel cell conditions will be presented. The results part is discussing fuel cell systems of different PTFE content which represent different ageing situations. Several approaches to analyse the simulations are presented and discussed. The article will be completed by a conclusions and outlook section.

2. Monte Carlo model

2.1. Description of the MC model

In contrast to the commonly known MC models, the model presented in the following does not work on the molecular level, but on the μm scale. MC models working on the molecular scale often use a (N, V, T)-ensemble to simulate a system at equilibrium. This

means that using a constant number of particles N, volume V and temperature T, the system explores the microscopic phase space in a way that average values gained from the simulation correspond to the values for the macroscopic thermodynamic equilibrium state.

The model presented here is grid-based with a voxel size of $5\,\mu m \times 5\,\mu m \times 5\,\mu m$. The lattice sites can be allocated with

- fibre material: graphite or PTFE;
- liquid water;
- "nothing" (gas phase not explicitly included);

Within the model periodic boundary conditions are applied in all directions of space. These boundary conditions can be lifted by walls delimiting the system. The wall particles do not have any interaction to the water droplets.

During a MC iteration, each water-occupied voxel is chosen once in random order for a tentative move, referred to as single MC step in the following. One free position among the six next neighbour voxels is randomly selected and the energy of the new and the old state are calculated. These interactions between the occupied voxels are modelled as pair interactions. The values of the interactions are based on surface energies. For the water–water interactions, $-72\,mN\,m^{-1}$ at 20°C are used. Temperature dependence of the value is taken into account via

$$E_{H_2O} = 0.07275\left(1 - 0.002\left(\frac{T}{K} - 291\right)\right).$$

For graphite–water $-95\,mN\,m^{-1}$ and for PTFE–water $+30\,mN\,m^{-1}$ have been estimated. The energy of a given state is calculated taking into account all occupied neighbouring positions of the voxel under consideration. Direct neighbours are fully counted, whereas for diagonal neighbours a weighting factor of $1/r^6$ is applied. The resulting energy is converted into a molar energy.

As usually, the total energy difference ΔE of the possible new energy to the old state determines the acceptance probability for the MC step via the Boltzmann factor

$$\exp\left(-\frac{\Delta E}{RT}\right). \quad (1)$$

Hereby, T is the absolute temperature and R denotes the universal gas constant. If the energy difference ΔE has a negative value, the factor is bigger than 1 and the MC move is accepted. If ΔE is positive, the exponent is smaller than 1 and a random number between 0 and 1 is calculated. If the Boltzmann factor is larger than this random number, the MC move is accepted. Otherwise, the old state of the system is preserved. In both cases, the iteration continues with the random selection of the next water-occupied voxel. The pseudo random number generator used within our model is the MT19937 'Mersenne Twister' from the Gnu Scientific Library (GSL) (for further information, see [39]).

2.2. Steady state

An operating fuel cell cannot be adequately described by a system in thermodynamic equilibrium. Hence, real FC operating conditions need to be approximated by other means. FC operation at constant current and flow rates can be characterized as a steady state. But as within the framework of a MC simulation, there is no meaningfull definition of the term 'time', also the concepts of current and flow cannot be directly applied. Therefore, we have developed a method to mimic steady state conditions within a MC simulation.

Real cell operating conditions employing constant current and flow rates correspond to a constant amount of water being transported through the GDL and then being removed by the gas flow through the channel structure within a given time span. Within the context of our model, this situation can be represented by enforcing a certain number of water 'particles' to be created (source) or destroyed (sink), respectively, in different regions of the system. Hereby, the aim is to reach a state in which the *average* number of water particles created and destroyed during a MC iteration reaches an *equal* and *constant* value. To describe a certain number of events *per iteration*, the term 'rate' is used in the following, although we are aware that this implies a re-definition of an established time-related concept which bears the danger of causing confusion.

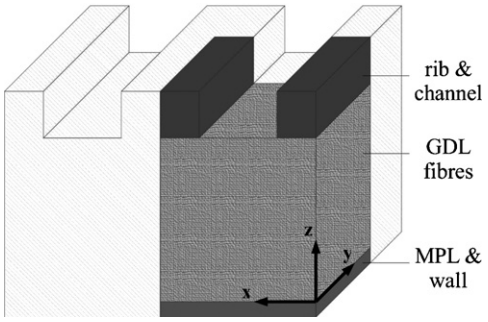

Fig. 1. Region of a fuel cell which is explicitly treated by the MC model.

To simulate a cathodic GDL within a FC in operation, the water source is located within the MPL to mimic water production at the reaction layer. Water creation is again a mainly random process taking place at free voxels within the MPL pores, governed by a certain creation probability. Nevertheless it is influenced to some extend by the water coverage of the surroundings. Water annihilation only takes place within the channel to mimic water removal by the gas flow there. Only water particles having a surface towards free space can be annihilated, again governed by a certain predetermined probability. Both predetermined probability values do not have a direct meaning, many combinations of values may lead to the same converged rate.

Besides the requirement of reaching such a converged source and sink rate, the usual condition for MC simulations that the mean number of accepted MC steps per iteration should be converged is taken as a further criterion. Additionally, the fraction of pore space in the inner-GDL region which is occupied by water is required to be constant. This quantity will be denoted as inner-GDL hydration in the following. If all three conditions are fulfilled, the state of the system shall be denoted as steady-state.

2.3. Handling of porous structures

Fig. 1 illustrates the part of the fuel cell explicitly represented within the MC model. As can be seen from the picture, not the complete fuel cell is modelled, but only the cathode side including the channel, the GDL and parts of the ribs of a flowfield.

The GDL fibre structure can be generated within the model employing an algorithm based on random growth processes. GDL fibres with a thickness of $10\,\mu m$ are grown in random directions until a maximum length or an obstacle is reached. Consequently, fibre intersections are avoided. Fibres are generated until a given porosity value is reached (porosity value: 76% within this study). For the GDL calculations presented in the following, a 'paper-like' structure is generated by preferring fibre growth within the xy-plane over the z-direction. Additionally, a MPL model consisting of hydrophobic (PTFE) material of arbitrary density is added.

As an additional feature, an interface to enable both importing of an externally generated structure, e.g. originating from adequate postprocessing of tomography data (e.g. reconstructed from synchrotron tomography data), and reading of program generated structures has been defined. The latter feature can be used to sys-

tematise simulation studies by using the same basic structure for all runs. This enables to compare model runs with different PTFE content as described in the following Section 3.

As the simulation box only covers a small section within the flowfield, periodic boundary conditions are applied in x and y directions, whereas the system is delimited by a wall in z-direction. Though, simulating realistic dimensions for the channel would impose too high computational effort, so the dimensions in x and y directions have to be reduced, whereas thickness has a realistic value. The following case study always uses a system size of $50 \times 50 \times 58$ voxels, i.e. $250\,\mu m \times 250\,\mu m \times 290\,\mu m$. Material compression below the ribs can also be reflected, a value of 20% compression is applied in the following.

3. Results

3.1. Simple systems in equilibrium

For testing and validating the MC model, a few simple test cases were studied at constant N, V and T. At first, a random water distribution in free space with zero gravity was generated. Gravity can be neglected due to the fact that the surface energy values are by several orders of magnitude larger than gravity. When the equilibrium state is reached, a single water drop is formed; this geometry minimizes the surface energy and is the one which should be expected from the physics of the system. Furthermore water behaviour on hydrophilic and hydrophobic material was studied. In equilibrium the water drop adsorbs to the preferable, hydrophilic material and forms a contact angle below 90° to the solid surface. In summary, the basic physical behaviour of liquid water as drop formation and behaviour against hydrophilic and hydrophobic material is reflected correctly.

3.2. GDL ageing

As mentioned in Section 1, two mechanisms are deemed to be responsible for GDL degradation: changes of the wetting behaviour due to PTFE loss and structural changes caused by mechanical effects (e.g. compression below the ribs). To model the effect of PTFE loss, several systems with decreasing PTFE content were set up, namely 85% PTFE coverage as model for a new GDL, and 75%, 65% and 55% PTFE coverage to represent different stages of ageing. PTFE coverage in our case means the fraction of fibre surface covered by PTFE, not the fraction of the total weight. The latter value is sometimes given by GDL manufacturers, but the direct relation to the surface coverage remains unclear. Thus we have chosen to take fraction of PTFE covered surface as input parameter. As a general scheme to set up a GDL structure for different MC simulation runs, first the pure carbon 'backbone' of fibres is generated (see Fig. 2(a)). The resulting setup constitutes the basic structure which can be reused for all simulations. Fig. 2(b) and (c) show a 85% PTFE coverage and a 55% PTFE coverage for the given backbone structure. For all runs within the study, the number of MC iterations after reaching the steady state, i.e. those which are used for analysis, is about 3×10^6. The converged source and sink rates are reaching the same value in all cases.

Snapshots of the resulting water distribution are shown in Fig. 3(a) and (b) for PTFE contents of 85% and 55%. In the case of 85% PTFE content, one can only find a few water drops (represented by blue color) within the GDL. Some water can also be found on the channel walls and within the channel. In contrast, regarding the snapshot of the GDL featuring a PTFE coverage of 55%, all free pores of the GDL seem to be filled with water and in addition the number of water particles on the channel walls and within the channel has increased. Water drops levitating within the channel should not be interpreted as such. Although they can be observed in the simulation snapshots, they correspond to energetically unfavourable, though possible, configurations. Under real two-phase flow conditions, water would be immediately removed by the gas flow within the channel. As can be seen in Section 3.3, they completely disappear during statistical averaging, as should be expected. Consequently, they are irrelevant for the water distribution resulting from the simulations.

As a first deeper analysis, the mean trial move acceptance and the inner hydration for different PTFE contents are considered. The trial move acceptance is formed as a mean value of the accepted MC moves per MC iteration (see Fig. 4(a)). The higher the PTFE content, the more moves are accepted. The number of accepted moves on the one hand depends on the number of water particles within the GDL, on the other hand on the material properties. The more water particles are present within the GDL, the less MC moves are possible because of the lower probability to find a free space to move to. A higher value of the acceptance rate also means that water particles move more frequently, cf. Section 3.3.

Fig. 4(b) represents the percentage of lattice sites occupied with water within the GDL. As could be expected, the water content within the inner GDL region strongly increases with decreasing PTFE content. Notably, going from 85% to 65%, the value roughly doubles for each step. In contrast, between 65% and 55% teflon coverage, an increase of over 300% can be observed. This feature will be analysed in detail in Section 3.3.

3.3. Analysis of water clustering and connectivity

To gain further insight into the structure of the water phase within the simulated GLD material and to be able to assess its possible impact on fuel cell operation, both finding a measure for the mean properties (i.e. ensemble average) of the water phase and characterizing its geometric structure are required. For the first task, one rather obvious approach is to calculate for each voxel the probability of being occupied by water during the steady state simulations. By defining a limit above which a voxel should be regarded as on average occupied by water, a mean water distribution can be derived.

Yet, though this enables visualization which helps to get an impression on how the GDL material is being filled by water, further consideration of the internal structure of the water phase is necessary to be able to quantify and rank its properties. One interesting question is whether the water is distributed approximately equally over the available empty space, or if it rather forms small or even big clusters and how these are interconnected. This information can be used to understand why routes of gas transport may be blocked or, on the other hand, water connections bridging the fibre structure and forming routes of water transport to the channel may be formed.

The so-called Hoshen–Kopelman-algorithm [40] provides a commonly used tool to analyse cluster structures. Its rationale is to analyse whether particles, i.e. water-occupied voxels in this case, have neighbours of the same material, i.e. likewise water-occupied voxels. Particles which are connected in this way are assigned to belong to the same cluster, which in the end results in a cluster map containing information on the total number of clusters in the system, the respective size of each cluster and which water-occupied voxels belong to it.

To relate the water clustering properties to the PTFE load, i.e. the presupposed ageing effect, a Hoshen–Kopelman-analysis of several snapshots from each steady state simulation for the different PTFE coverage values has been performed. A typical example for each coverage is shown in Fig. 5. To visualize the Hoshen–Kopelman results, each distinguishable cluster is assigned a different color.

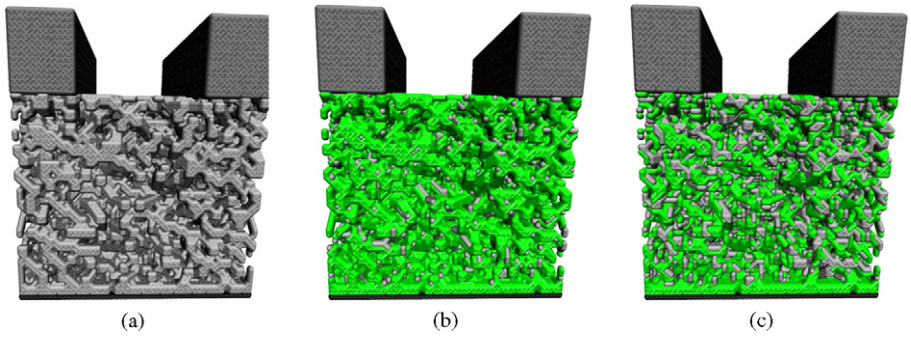

Fig. 2. Pure carbon 'backbone' structure (a) and two different PTFE loadings (b) 85% PTFE, and (c) 55% PTFE. Grey represents the graphite fibres and the flowfield ribs consisting of graphite. PTFE covered voxels are displayed in green color. (For interpretation of the references to color in this figure legend, the reader is referred to the web version of the article.)

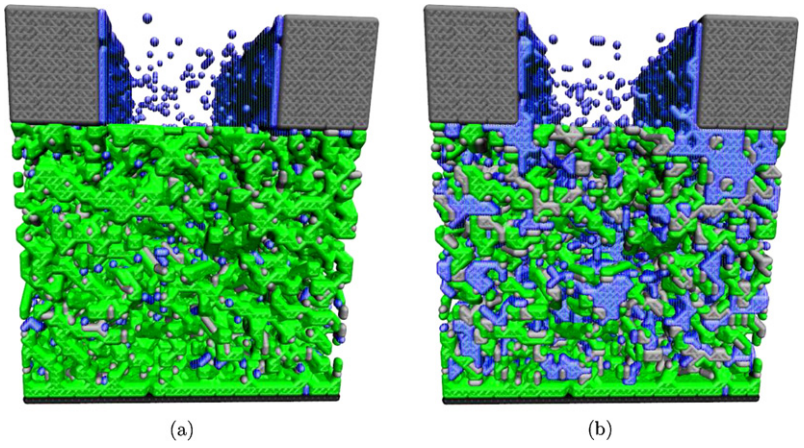

Fig. 3. Water distribution for different PTFE loadings. Blue represents the water, grey the graphite fibres and the flowfield ribs and green the PTFE. (a) 85% PTFE coverage; (b) 55% PTFE coverage. (For interpretation of the references to color in this figure legend, the reader is referred to the web version of the article.)

As can be seen from Fig. 5(a), which represents a new GDL, the overall quite low water content within the GDL, cf. Fig. 4(b), is apparently randomly distributed over the pore space in small clusters. The only big clusters that can be identified constitute a water film on the hydrophilic channel walls. The latter to some extend reach under the channel ribs, where first larger agglomerations of water clusters can be observed.

Going to the teflon coverages below 85% modelling aged material, as can be expected one finds an increasing water occupation with decreasing PTFE content. At 75%, especially the water clusters residing under the flowfield ribs grow remarkably. This trend is affirmed for 65% together with the emergence of larger clusters in the inner regions of the GDL. Still, they remain separated and seem randomly distributed.

In contrast to the continuous increase so far, going to 55% brings along an escalating water content, Fig. 4(b). Whereas for the other ageing grades the inner-GDL water content roughly doubled per 10% points decrease of PTFE, we now see an increase to above 300%. As Fig. 5(d) shows this already corresponds to a flooding of large parts of the inner-GDL volume resulting in a water phase which is mostly continuous, i.e. mainly consists of one large cluster. Of course, although this liquid water content still should leave free pore space for the gas flow, such a large cluster extending over the whole GDL area already constitutes a major obstacle. Furthermore,

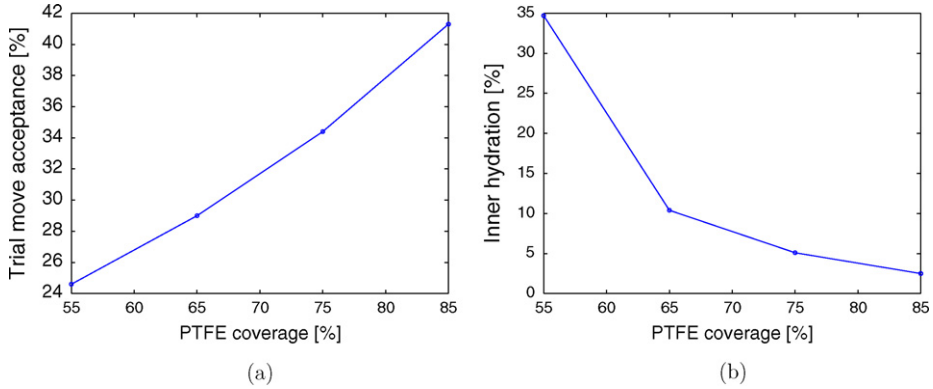

Fig. 4. The trial move acceptance over PTFE content (a) represents the percentage of accepted moves. The inner hydration over PTFE content (b) indicates the percentage of lattice sites occupied with water.

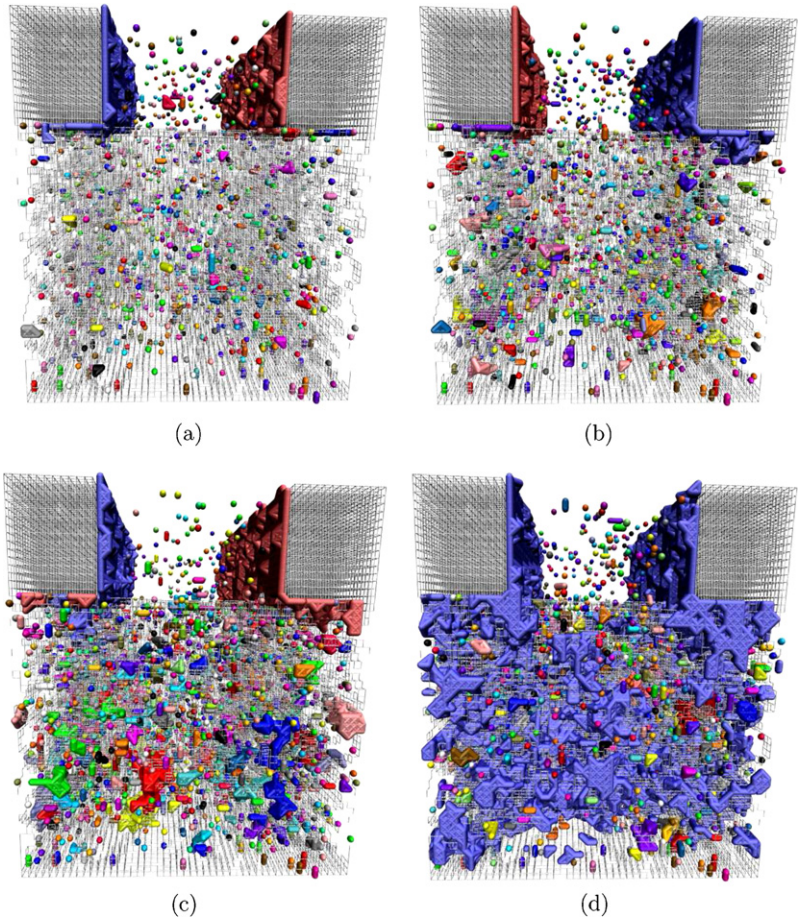

Fig. 5. Formation of water clusters for different PTFE content (multi-colored), ribs and fibres are displayed as grey scaffold; snapshots of single MC configurations. (a) 85% PTFE; (b) 75% PTFE; (c) 65% PTFE; (d) 55% PTFE.

as liquid water within the GDL in turn is suspected to enhance GDL degradation [11], one may expect a self-enhancing of ageing from here on.

Of course, the argumentation presented so far is based on simulation snapshots, and meaningful conclusions from MC simulations should be based on average values representing the statistics of the ensemble. But for the case of water distribution, the latter are not as easily interpretable as, for e.g. values of energy, etc. which are commonly averaged. It is rather easy to define a mean water distribution, e.g. by defining that all voxels which feature a occupation probability of 70% or higher over the respective steady-state simulation should be regarded as water-occupied. But on the other hand, one must bear in mind that a water drop which is alternately changing its geometric location between two voxels would not contribute to the distribution defined this way, although it is present at nearly the same place in all configurations. On the other hand, when finding occupation probabilities of over 70% over ample regions of space, one can be rather sure, that this corresponds to a significant water agglomeration that can be located at this spot. If furthermore the findings from such mean values are consistent with representative screenshots as presented before and integrated data as the distributions presented later, they can be deemed to be meaningful.

Fig. 6 features such water cluster data for a occupation probability of over 70% as described just above. Additionally, again a Hoshen–Kopelman analysis has been performed according to which different clusters are drawn using different colors as for the snapshot cases depicted above. As mentioned, by definition this average water occupation tends to contain only that part of the overall water content of the steady-state simulations which remains stationary. This can be clearly seen from a comparison of Figs. 5(a) and 6(a): Though the total water content is constant throughout the simulation, the numerous small water clusters visible in the snapshot picture have no counterpart in Fig. 6(a). Here, one just finds the water film on the channels walls as known from above and some water occupation below the flowfield ribs. This means that most of the liquid water content within the GDL is not only dispersed over the structure, but also the resulting small clusters are rather mobile within the simulation, i.e. many configurations of similar energy can be realized by the system.

The small pillars at the bottom part of Fig. 6(a), which are also visible in the other figures, correspond to pores within the MPL, which are used to model water transport from the reaction layer towards the fibre structure; this is rather a technical feature, as due to the different pore size ranges of MPL and fibre structure, simulating the MPL geometry on the same lengthscale is not feasible. Consequently, they should not be over-interpreted.

Going towards 75% and 65% PTFE coverage, obviously more of the water clusters become resident; stationarity appears to be a feature which is related to increasing cluster size. Furthermore, the water agglomerations below the flowfield ribs as monitored from the snapshot examples can be confirmed. Regarding 55% teflon coverage, the formation of one single and – compared to the other cases – extraordinary big connected water cluster can be validated. Even for the relatively demanding criterion of at least 70% probability, it continuously connects the MPL region to the channel ribs. Overall, one can state that the results of the occupation probability analysis back and clarify the findings from the snapshot examples. Furthermore, they enable the interpretation in terms of cluster mobility.

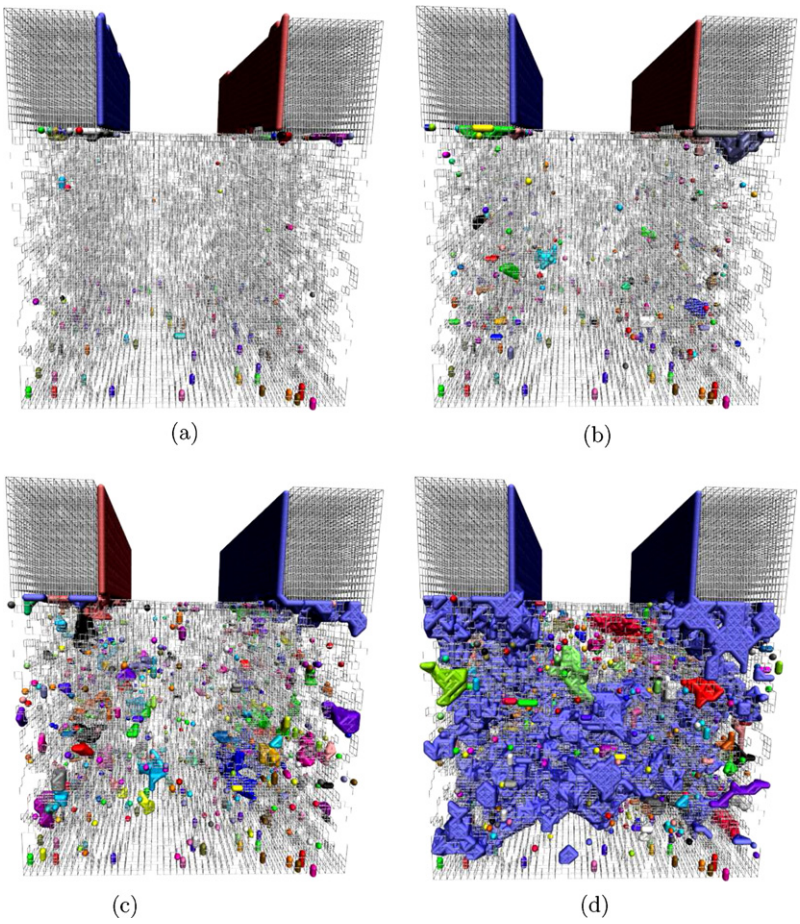

Fig. 6. Mean hydration for different PTFE content values. Voxels featuring at least 70% probability of water occupation are shown as water, cluster affiliation represented by multi-coloring. (a) 85% PTFE; (b) 75% PTFE; (c) 65% PTFE; (d) 55% PTFE.

This water cluster formation within the MC model appears to be in accordance with results from visualization experiments. Hartnig et al. [41] show a tomogram of a water filled sample of a GDL. The three different phases, the fibre material, the water filled pores and the free pores are presented together, and additionally every phase is shown in an extra picture. Regarding the water filled pores, one can see many small water clusters formed within the GDL material.

Regarding further experimental results [37,38], one can find water cluster formation below the ribs within the GDL material. However, one has to take into account that this experimental visualization of the water within a GDL was done for a new GDL material at different current densities. The higher the current density, the more water clusters are formed. As within this study, we are focussing on variation of the PTFE content, we cannot directly compare our results with these experimental ones. Nevertheless, one can conclude that our model and the experiments agree insofar that water cluster formation starts below the ribs.

A further aspect which can be considered employing the Hoshen–Kopelman analysis is the distribution of cluster sizes over the steady-state simulations. It can be calculated from the cluster map data which contains for each cluster the respective size averaging over different configurations. Due to the quite high computational effort for the Hoshen–Kopelman algorithm, this could only be done 30 times within each steady-state run consisting of 3×10^6 iterations. Nevertheless, the data should be representative enough to provide relevant information.

Fig. 7 features the corresponding cluster size distribution density curves for the different PTFE coverage values. There are two characteristic trends which can be monitored here: First, the maximum cluster size changes drastically with decreasing hydrophobicity. This is especially evident between 65% PTFE and 55% PTFE, where the increase in size amounts one order of magnitude, from 10^3 to 10^4. This corresponds well to the volatile behaviour between these two ageing states as depicted above.

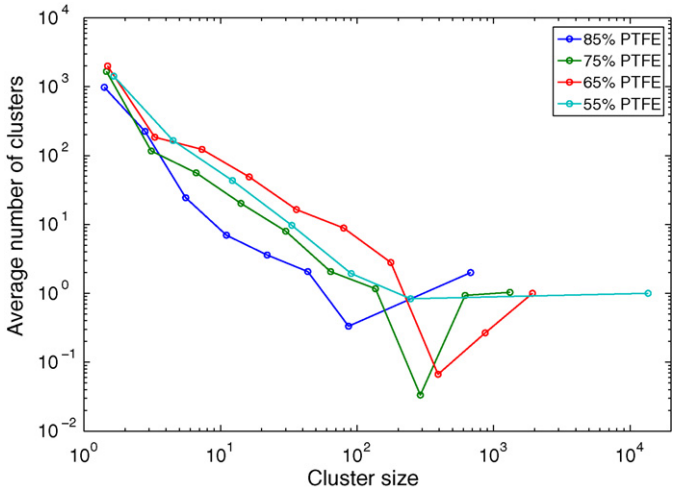

Fig. 7. Cluster size distributions for different PTFE coverage values. The cluster size is given in voxels.

Second, in the size region between approximately 10 and 100 voxel, there is a clear trend to increase the number of these mid-size clusters going from 85% PTFE to lower contents. The only exception is 55% PTFE, where the very large cluster may 'absorb' many of the smaller ones.

4. Conclusions and outlook

As the properties of the water household and the degradation mechanisms of fuel cell GDLs are still not well understood, there is a strong need also for theoretical models suitable to tackle this problem. The MC model presented in this work provides a useful tool to investigate the relevant processes concerning the distribution of liquid water within the GDL on the μm scale. Although there are well-established models in the field, it can serve as a valuable completion due to its special features and the comparatively low computational effort.

The results presented in this work show a clear influence of the PTFE coverage upon the amount of water residing within the GDL fibre structure and the structural properties of the water phase observed. First, with decreasing PTFE coverage more and also larger water clusters are formed, but upon reaching a critical value, the behaviour changes to the formation of a comparatively very tall cluster geometrically connecting all GDL regions. This may be critical for fuel cell operation, and could on the other hand further accelerate GDL ageing in the sense of a self-enhancing mechanism.

Experimental validation of the results can be directly achieved by comparison to in situ observations using, e.g. synchrotron tomography or other imaging techniques, but unfortunately to the best of our knowledge, no appropriate in situ data on aged material is available for comparison. First appraisal of the results appears promising, and in-deep comparison is planned for the future. Furthermore, simulations employing GDL structures obtained by reconstruction of tomography data and larger simulation cells are going to be performed to reach further improvement in the description of real systems.

Acknowledgements

The authors wish to thank E. Santos, W. Schmickler and H. Haßfeld for helpful discussions. Financial support by the EU project DECODE (Understanding of Degradation Mechanisms to Improve Components and Design of PEMFC, grant no. 213295) within the Seventh Framework Programme is gratefully acknowledged.

References

[1] F. De Bruijn, V. Dam, G. Janssen, Fuel Cells 8 (2008) 3–22.
[2] W. Schmittinger, A. Vahidi, Journal of Power Sources 180 (2008) 1–14.
[3] J. Wu, X. Yuan, J. Martin, H. Wang, J. Zhang, J. Shen, S. Wu, W. Merida, Journal of Power Sources 184 (2008) 104–119.
[4] L. Jörissen, W. Lehnert, J. Garche, W. Tillmetz, Materials Science Forum 539-543 (2007) 1303–1308.
[5] M. Schulze, N. Wagner, T. Kaz, K. Friedrich, Electrochimica Acta 52 (2007) 2328–2336.
[6] S. Knights, K. Colbow, J. St-Pierre, D. Wilkinson, Journal of Power Sources 127 (2004) 127–134.
[7] B. Thoben, A. Siebke, Journal of New Materials for Electrochemical Systems 7 (2004) 13–20.
[8] A. Bazylak, D. Sinton, Z. Liu, N. Djilali, Journal of Power Sources 163 (2007) 784–792.
[9] S. Escribano, J. Blachot, J. Ethève, A. Morin, R. Mosdale, Journal of Power Sources 156 (2006) 8–13.
[10] S. Maass, F. Finsterwalder, G. Frank, R. Hartmann, C. Merten, Journal of Power Sources 176 (2008) 444–451.
[11] J. Xie, D. Wood, D. Wayne, T. Zawodzinski, P. Atanassov, R. Borup III, Journal of the Electrochemical Society 152 (2005) A104–A113.
[12] Langlebige PEFC als Voraussetzung für eine Wasserstoffenergiewirtschaft, Technical Report, BMWi, German Federal Ministry of Economics and Technology, 2000–2005.
[13] P. Nguyen, T. Berning, N. Djilali, Journal of Power Sources 130 (2004) 149–157.
[14] Z. Wang, C. Wang, K. Chen, Journal of Power Sources 94 (2001) 40–50.
[15] D. Wolf-Gladrow, Lattice-gas Cellular Automata and Lattice Boltzmann Models: An Introduction, Springer Verlag, 2000.
[16] I. Fatt, Transactions of AIME 207 (1956) 144–181.
[17] M. Allen, D. Tildesley, Computer Simulation of Liquids, Oxford University Press, Oxford, 1990.
[18] D. Frenkel, B. Smit, Understanding Molecular Simulation: From Algorithms to Applications, Academic Press, 2002.
[19] D. Rapaport, The Art of Molecular Dynamics Simulation, Cambridge University Press, 2004.
[20] J. Haile, Molecular Dynamics Simulation: Elementary Methods, John Wiley & Sons, Inc., New York, NY, USA, 1992.
[21] N. Metropolis, A. Rosenbluth, M. Rosenbluth, A. Teller, E. Teller, et al., The Journal of Chemical Physics 21 (1953) 1087–1092.
[22] R. Paul, H. Rieger, The Journal of Chemical Physics 123 (2005) 024708.
[23] M. Hashemi, M. Sahimi, B. Dabir, Physica A 267 (1999) 1–33.
[24] S. Jain, M. Acharya, S. Gupta, A. Bhaskarwar, Computers & Chemical Engineering 27 (2003) 385–400.
[25] J. Zalc, S. Reyes, E. Iglesia, Chemical Engineering Science 58 (2003) 4605–4617.
[26] J. Abel, A. Kornyshev, W. Lehnert, Journal of the Electrochemical Society 144 (1997) 4253–4259.
[27] M. Van Doormaal, J. Pharoah, International Journal for Numerical Methods in Fluids 59 (2008) 75–89.
[28] M. Tomadakis, S. Sotirchos, AIChE Journal 37 (2004) 74–86.
[29] F. Transvalidou, S. Sotirchos, AIChE Journal 42 (2004) 2426–2438.
[30] S. Torquato, Random Heterogenous Materials: Microstructure and Macroscopic Properties, Springer Verlag, New York, 2002.
[31] K. Mecke, D. Stoyan (Eds.), Statistical Physics and Spatial Statistics. The Art of Analyzing and Modeling Spatial Structures and Pattern Formation, vol. 554, Springer, Berlin, 2000.
[32] K. Mecke, D. Stoyan (Eds.), Morphology of Condensed Matter: Physics and Geometry of Spatially Complex Systems (Lecture Notes in Physics), Springer Verlag, Berlin, 2002.
[33] D. Stoyan, W. Kendall, J. Mecke, Stochastic Geometry and Its Applications, John Wiley & Sons, Chichester, New York/Brisbane, Toronto/Singapore, 1987.
[34] F. Zhang, X. Yang, C. Wang, Journal of the Electrochemical Society 153 (2006) A225–A232.
[35] I. Manke, C. Hartnig, M. Grünerbel, J. Kaczerowski, W. Lehnert, N. Kardjilov, A. Hilger, J. Banhart, W. Treimer, M. Strobl, Applied Physics Letters 90 (2007) 184101.
[36] D. Spernjak, S. Advani, A. Prasad, Journal of the Electrochemical Society 156 (2009) B109–B117.
[37] I. Manke, C. Hartnig, M. Grünerbel, W. Lehnert, N. Kardjilov, A. Haibel, A. Hilger, J. Banhart, H. Riesemeier, Applied Physics Letters 90 (2007) 174105.
[38] C. Hartnig, I. Manke, R. Kuhn, N. Kardjilov, J. Banhart, W. Lehnert, Applied Physics Letters 92 (2008) 134106.
[39] M. Matsumoto, T. Nishimura, ACM Transactions on Modeling and Computer Simulation (TOMACS) 8 (1998) 3–30.
[40] J. Hoshen, R. Kopelman, Physical Review B 14 (1976) 3438–3445.
[41] C. Hartnig, R. Kuhn, P. Kruge, I. Manke, N. Kardjilov, J. Goebbels, B. Muller, H. Riesemeier, MP Materials Testing (2008) 50.